Applied Catalysis B: Environmental 263 (2020) 118227

Contents lists available at ScienceDirect

Applied Catalysis B: Environmental

journal homepage: www.elsevier.com/locate/apcatb

Enhancement of photocatalytic NO_x abatement on titania *via* additional metal oxide NO_x-storage domains: Interplay between surface acidity, specific surface area, and humidity

Mustafa Çağlayan[a,1], Muhammad Irfan[a,c], Kerem Emre Ercan[a], Yusuf Kocak[a], Emrah Ozensoy[a,b,*]

[a] Chemistry Department, Bilkent University, 06800, Bilkent, Ankara, Turkey
[b] UNAM-National Nanotechnology Center, Bilkent University, 06800, Ankara, Turkey
[c] Nanoscience and Catalysis Department, National Centre for Physics, 44000, Islamabad, Pakistan

ARTICLE INFO

Keywords:
NO_x abatement
Photocatalytic NO_x oxidation-storage (PHONOS)
Titania
Calcium oxide
Alumina
$DeNO_x$ catalysts

ABSTRACT

In this work, we propose a simple and effective preparation procedure to obtain ternary mixed oxides composed of titania (TiO_2, P25), alumina (γ-Al_2O_3) and calcium oxide (CaO) functioning as efficient photocatalytic NO_x oxidation and storage (PHONOS) catalysts that are capable of facile NO_x abatement under ambient conditions in the absence of elevated temperatures and pressures with UVA irradiation. In this architecture, titania was the photocatalytic active component and CaO and/or γ-Al_2O_3 provided NO_x storage domains revealing dissimilar specific surface areas (SSA) and surface acidities. We show that photocatalyst formulation can be readily fine-tuned to achieve superior photocatalytic performance surpassing conventional P25 benchmark in short (1 h) and long term (12 h), as well as humidity-dependent photocatalytic tests. We demonstrate the delicate interplay between the surface acidity, SSA and humidity and provide detailed mechanistic insights regarding the origin of photocatalytic activity, selectivity and deactivation pathways.

1. Introduction

Environmental pollution is one of the major challenges faced by the modern human societies. Anthropogenic air pollutants such as nitrogen oxides (NO_x) not only induce ozone production in troposphere and cause acid rain, but also severely affect human respiratory and immune systems [1,2]. Environmental protection agencies have set a recommended value of $\leq$ 0.2 ppm for NO_x emissions which is exceeded routinely in urban settings in Europe [3]; calling for an urgent need for more efficient and novel approaches for NO_x abatement. In conventional $DeNO_x$ technologies associated with stationary (*e.g.* heating systems, power plants *etc.*) and mobile sources (marine, aerial, and land transportation/construction vehicles), NO_x abatement is typically aimed to be accomplished at the source of the NO_x generation using thermal catalytic technologies (*i.e.* selective catalytic reduction/SCR and NO_x storage and reduction/NSR) at elevated temperatures [4–7]. As a result of the frequent violations of transportation-based NO_x emission limits by numerous car manufacturers in Europe, on-board NO_x emissions have been reported to be up to 16 times higher than those values measured in test stands [8]. It is estimated that such violations are causing annually *ca.* 5000 premature mortalities in Europe [8].

Therefore, an important challenge is the abatement of gaseous NO_x species after their point of origin in urban settings under ambient conditions (*i.e.* at room temperature and at atmospheric pressure). In this regard, Photocatalytic Oxidative NO_x Storage (PHONOS) is an attractive alternative [9–12]; which can exploit readily available solar radiation under ambient conditions and store airborne NO_x in the solid state. This approach has been already implemented in advanced construction materials to combat urban NO_x pollution [13,14], using mainly titanium dioxide (TiO_2) based photocatalysts. TiO_2 is the most widely used semiconductor for the photocatalytic decomposition of gaseous and liquid phase pollutants as it is abundant, cost-efficient, chemically and thermally stable, hydrophilic, non-toxic, and is also capable of oxidizing organic/inorganic species [15]. However, it has been reported that complete photocatalytic reduction of toxic NO_x species into harmless N_2 occurs only with an extremely limited extent on titania [16]. More importantly, in photocatalytic NO_x abatement applications, TiO_2 has a low selectivity towards NO_x storage in solid state and tends to oxidize NO (g) into a more toxic product, NO_2 (g),

* Corresponding author at: Chemistry Department, Bilkent University, 06800, Bilkent, Ankara, Turkey.
E-mail address: ozensoy@fen.bilkent.edu.tr (E. Ozensoy).
[1] Present Address: King Abdullah University of Science and Technology, KAUST Catalysis Center, Advanced Catalytic Materials, Thuwal, Saudi Arabia.

https://doi.org/10.1016/j.apcatb.2019.118227
Received 2 July 2019; Received in revised form 26 August 2019; Accepted 22 September 2019
Available online 26 September 2019
0926-3373/

which eventually slips into atmosphere [17]. Therefore, it is necessary to develop improved photocatalyst systems with high stability, efficiency and selectivity. Moreover, these prospective $DeNO_x$ materials should be abundant, accessible, easy to synthesize, stable, affordable and non-toxic in order to justify their implementation on a large scale.

In the current work, we focus on photocatalytic oxidation and storage of NO_x in the solid state in the form of nitrates and nitrites on photocatalyst surfaces containing CaO, Al_2O_3, and TiO_2 metal oxide mixtures. NO and NO_2 are two of the most predominant toxic species in atmospheric NO_x emissions. Electronic structures of NO and NO_2 molecules reveal a radical nature exhibiting electron deficiency due to unpaired valence electrons. Thus, they can function in an amphiphilic manner as Lewis acids and/or Lewis bases. For instance, NO_2 adsorbed on alkaline earth metal oxide surfaces can interact simultaneously with both Lewis basic sites such as O^{2-} (surf) as well as Lewis acidic sites such as M^{2+} (surf) forming nitrite and nitrate pairs which can interact in a synergistic (cooperative) fashion forming extremely stable co-adsorbed nitrate and nitrite species [18]. On alkaline earth metal oxide surfaces, adsorbed nitrate and nitrite species can also be formed as a result of an electron transfer between two adsorbed NO_2 species forming Lewis acidic NO_2^+ (surf) and Lewis basic NO_2^- (surf) species, with a high affinity toward O^{2-} (surf) or M^{2+} (surf) sites, respectively [18–20]. It was confirmed experimentally in earlier studies [21] that nitrites are formed during the earlier stages of NO_2 adsorption on alkaline earth metal oxide surfaces at room temperature; confirming the formation of nitrite-nitrate ion pairs [22]. Furthermore, *via* our former *in-situ* FTIR and temperature programmed desorption (TPD) studies [5–7,23–30], it has been demonstrated that during the NO_2 adsorption on titania, alumina and alkaline earth oxides at room temperature, nitrites are gradually converted into nitrates upon extended NO_2 exposure, yielding various types of surface nitrate species with moderate surface adsorption strength, as well as bulk-like nitrates with an extremely high adsorption strength on alkaline earth oxides.

Hence, relative surface acidity of a metal oxide surface is a critical factor governing the extent and strength of its interactions with gaseous NO_x species. It is well known that both Lewis and Brønsted surface acidities of calcium oxide, titania and alumina are ranked in the following increasing order CaO < TiO_2 (anatase) < δ-Al_2O_3 [31]. In other words, surface acidity of titania (*i.e.* the most commonly used photocatalyst in $DeNO_x$ applications) lies between the more basic CaO and the more acidic δ-Al_2O_3. Another crucial parameter influencing the NO_x adsorption and storage capacity of a metal oxide surface is the specific surface area (SSA) of the corresponding metal oxide. The most commonly utilized conventional commercial titania benchmark catalyst is P25 with a typical SSA of *ca.* 50 m^2/g, while SSA of typical γ-Al_2O_3 and CaO materials are *ca.* 200 m^2/g and 3 m^2/g, respectively (this work). Hence; CaO, Al_2O_3, and TiO_2 mixed metal oxides reveal an interesting playground for investigating the effects of surface acidity and SSA on photocatalytic NO_x oxidation and storage.

Furthermore; understanding the interplay between titania and CaO in photocatalytic $DeNO_x$ systems is quite important, since titania-based photocatalytic construction materials are also likely to contain natural Ca-based minerals such as CaO, $Ca(OH)_2$ and $CaCO_3$ (limestone) as additives. For instance, limestone content of typical cement binders can be as high as > 60 wt.% [32].

Interaction between titania and alumina in photocatalytic $DeNO_x$ systems is also worth investigating since, among different transitional alumina phases, γ-Al_2O_3 is the most widely used support material due to its superior chemical and thermal stability, high surface area and favorable surface acid/base properties [33]. In automotive emission control applications, γ-Al_2O_3 is frequently used as a $DeNO_x$ catalyst support material in three-way catalytic converter systems (TWC) and NSR systems. In NSR catalyst systems [6,7,23–26], although most of the NO_x is stored on various basic metal oxides (*e.g.* BaO) supported on alumina, γ-Al_2O_3 can also contribute to the total NO_x storage capacity of the catalytic systems by enabling the formation of surface nitrites and to a greater extent surface nitrates with different adsorption geometries (*e.g.* monodentate, bidentate or bridging nitrates) [34–38]. It is also very well known that nitrates formed upon NO_2 adsorption on the relatively acidic γ-Al_2O_3 surface reveal a significantly weaker adsorption strength than that of the nitrates formed on basic alkaline earth oxides upon NO_2 adsorption [6,7,23–26].

In former studies, we [5] as well as others (*e.g.* see the detailed discussion in Ref [39] about NO_2 adsorption on titania in the presence and absence of water investigated *via in-situ* FTIR spectroscopy) have spectroscopically demonstrated that both on TiO_2 and on TiO_2/M_xO_y binary oxide surfaces, oxidized NO_x species such as NO_2 (g) can readily undergo further disproportionation reactions forming various species such as adsorbed NO_2^- (nitrites), NO_3^- (nitrates), NO^+, HNO_3, HNO_2 *etc*. facilitating efficient NO_x storage at the solid-state.

However, NO (g) has a limited adsorption energy on many metal oxide surfaces compared to that of NO_2, hindering the direct storage of NO in the solid (adsorbed) state. Thus, for solid state NO_x storage, NO should be first oxidized to NO_2 and then subsequently stored on the available adsorption sites of the catalyst surface in the form of nitrites/nitrates. Although oxidation of NO can be done readily at elevated temperatures using precious metals, it cannot be efficiently achieved under ambient conditions due to kinetic limitations. However, this limitation can be overcome by designing a catalytic system including a photocatalytic NO oxidation component (*i.e.* TiO_2) which is coupled to NO_x storage domains (*i.e.* CaO and Al_2O_3). Along these lines, in the current work, we show that CaO, Al_2O_3 and TiO_2 containing mixed oxide surfaces can be exploited to perform efficient photocatalytic NO_x oxidation and storage, where TiO_2 surface domains provide the catalytic NO oxidation capability under ambient conditions, converting NO into NO_2, nitrites and nitrates, while CaO and Al_2O_3 components provide additional surface adsorption sites for non-catalytic storage of oxidized NO_x (Scheme 1). Note that rather than BaO, which is the most commonly used NO_x storage component in NSR catalytic formulations, we preferred to use CaO in the current work due to the higher cost and toxicity of the former material.

It is clear that the photocatalytic NO_x oxidation and storage (PHONOS) catalyst proposed in Scheme 1 is subject to eventual saturation and loss of activity due to the blocking of both catalytic (TiO_2) and non-catalytic (CaO or Al_2O_3) surface adsorption sites with NO_x oxidation products such as surface/bulk nitrites and nitrates [30,40]. This is also a frequently observed phenomenon in NSR catalysts, where the NO_x storage domains comprised of basic metal oxides such as BaO are eventually saturated with nitrates and lose their NO_x storage capacity. In such thermal catalytic systems, regeneration of the basic

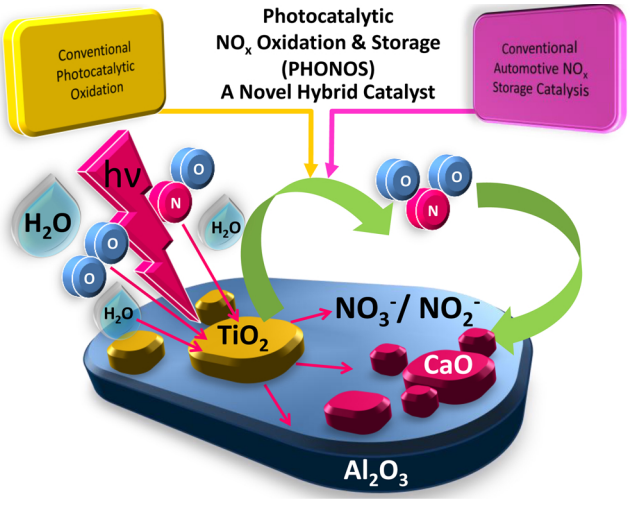

Scheme 1. Hybrid Photocatalytic NO_x Oxidation and Storage (PHONOS) catalyst concept with enhanced NO_2 capture and improved $DeNO_x$ selectivity.

metal oxide domains is accomplished *via* reduction of nitrates to nitrogen using external reducing agents (*e.g.* CO, NH_3, hydrocarbons, and H_2 *etc.*) through the assistance of precious metal (*e.g.* Pd, Pt) catalytic active sites within 200–450 °C. On the other hand, in principle, saturated or deactivated $DeNO_x$ photocatalysts can be readily regenerated with the help of water (*i.e.* rain, in case of outdoor applications or wet cleaning for indoor applications) at room temperature, which would dissolve and wash-off the surface nitrates and nitrites leaving behind regenerated surface sites available for further catalytic action as well as non-catalytic adsorption (NO_x storage). It should be noted that titania and alumina are not soluble metal oxides in ordinary aqueous systems (unless pH of the aqueous system is extremely low or extremely high, which would not be the case for the currently proposed water-based regeneration conditions). Thus, regeneration is not expected to deplete neither titania nor alumina contents of the photocatalyst formulation by dissolution. CaO can react with water to form $Ca(OH)_2$ which is also a sparingly soluble salt in water with a K_{sp} of *ca.* 5.5×10^{-5} at 298 K. Although this may lead to some performance loss (as demonstrated in our current work), a macroscopic loss of CaO due to interaction of water is also not presumable. On the other hand, NO_x species stored on CaO in the form of *e.g.* $Ca(NO_3)_2$ and $Ca(NO_2)_2$ are readily soluble in water and can be removed from the catalyst by washing with water. Considering the miniscule amount of surface $Ca(NO_3)_2$ and $Ca(NO_2)_2$ species that will be generated from ppb-level concentrations of atmospheric NO_x (g), a significant (*i.e.* macroscopic) loss of Ca-based salts upon nitrate regeneration with water is also not expected.

While this may be true, photocatalytic NO oxidation mechanisms also include adsorbed water molecules and surface hydroxyl/hydroxide functionalities as important players [41]. Therefore, in the current work, we also investigated the influence of adsorbed water (*i.e.* humidity) on the photocatalytic $DeNO_x$ efficiency of CaO, Al_2O_3, and TiO_2 metal oxide mixtures. Currently presented study reveals an extremely simple but an efficient methodology that can significantly enhance the photocatalytic NO_x abatement performance of commercial titania (P25) benchmark photocatalyst by providing detailed information on catalyst formulation and performance optimization, along with relevant mechanistic insight.

2. Materials and methods

Titanium (IV) oxide (P25, ≥99.5% trace metal basis) and calcium oxide (CaO, reagent grade) were purchased from Sigma-Aldrich. γ-Al_2O_3 (PURALOX SBa200, 200 m^2/g) was obtained from SASOL GmbH. All chemicals were used as received without further purification.

2.1. Preparation of CaO/P25 binary oxides

CaO was physically mixed with the benchmark photocatalyst P25 using a pestle and mortar. The resulting binary mixtures were labelled as 1Ca/Ti, 5Ca/Ti, 10Ca/Ti, 25Ca/Ti, 50Ca/Ti and 75Ca/Ti. Here, Ca and Ti stand for CaO and P25 (TiO_2), respectively, while the number before Ca represents the weight percent of the CaO component in the binary mixture.

2.2. Preparation of γ-Al_2O_3/P25 binary oxides

Puralox SBa200 γ-Al_2O_3 was physically mixed with P25 using a pestle and mortar. The resulting binary mixtures were labelled as 10Al/Ti, 30Al/Ti, 50Al/Ti, 70Al/Ti and 90Al/Ti. Here, Al and Ti stand for γ-Al_2O_3 and P25 (TiO_2), respectively, while the number before Al represents the weight percent of the γ-Al_2O_3 component in the binary mixture.

2.3. Preparation of CaO/γ-Al_2O_3/P25 ternary oxides

Since the binary Al/Ti sample with the optimum performance was obtained for the 70Al/Ti catalyst, this catalyst was further enriched with CaO in an attempt to improve the photocatalytic performance and achieve a more affordable photocatalyst formulation by decreasing the titania content of the photocatalyst for large scale applications. Along these lines, in order to keep the relative weight percent of γ-Al_2O_3 and P25 (TiO_2) components constant at 70/30 = 2.33 in the physically mixed ternary mixture, we added CaO to the Al/Ti binary mixtures such that the CaO content of the ternary mixture was 1, 5, 10, 25, 50, 70 and 90 wt.%. These samples were labeled as 1Ca/69Al/30Ti, 5Ca/66Al/29Ti, 10Ca/63Al/27Ti, 25Ca/53Al/22Ti, 50Ca/35Al/15Ti, 70Ca/21Al/9Ti and 90Ca/7Al/3Ti, where the numbers in the acronyms before each element represent the corresponding weight percentile of each metal oxide component (*i.e.* CaO, Al_2O_3 and TiO_2, respectively) in the ternary mixture.

2.4. Structural characterization

Crystal structures of the synthesized materials were analyzed using a Rigaku Miniflex X-Ray Diffractometer, equipped with Cu Kα radiation operated at 30 kV, 15 mA and 1.54 Å. Samples were pressed onto a standard-sized glass slides and scanned in the 2θ range of 10-80° with a step width 0.01° s^{-1}. The Brunauer-Emmett-Teller (BET) specific surface area (SSA) measurements of the prepared photocatalysts were carried out using nitrogen adsorption–desorption isotherms obtained with a Micromeritics 3Flex surface area and pore size analyzer. Prior to SSA analysis, all samples were outgassed in vacuum for 2 h at 150 °C. *In-situ* Fourier transform infrared (FTIR) spectroscopy experiments involving NO_2 and pyridine adsorption and *ex-situ* FTIR experiments immediately after PHONOS catalytic activity tests were performed in two different custom-made spectroscopic batch reactors containing a Bruker Tensor 27 transmission FTIR spectrometer with a mercury-cadmium-telluride (MCT) detector. One of these reactors was also equipped with a quadruple mass spectrometer (QMS, SRS RGA 200) for NO_x temperature programmed desorption (TPD) experiments. Details of the *in-situ* FTIR and TPD experiments are provided in the supporting information section. Scanning electron microscopy (SEM) and energy dispersive X-ray analysis (EDX) measurements were performed using an electron microscope (FEI Quanta 200) equipped with a field emission gun (FEG) and an EDX detector.

2.5. Photocatalytic activity measurements

The photocatalytic $DeNO_x$ experiments were performed at room temperature in flow mode by considering the experimental requirements that were reported in the ISO 22197-1 standard [42]. Inlet gas mixture that was introduced to the reactor (Fig. S**1**) contained 0.750 standard liters per minute (SLM) N_2 (g) (purity: 99.99%, Linde GmbH), 0.250 SLM O_2 (purity: 99%, Linde Gm bH) and 0.010 SLM NO (100 ppm NO (g) diluted in balance N_2 (g), Linde GmbH). In order to obtain the gas flow values given above, mass flow controllers (MFCs, MKS1479A for N_2 (g) and O_2 (g) and Teledyne HFC-202 for NO (g) diluted in N_2 (g)) were utilized so that the typical total gas flow over the photocatalyst was stabilized at 1.010 SLM ± 0.05 SLM, where the NO (g) content of the inlet gas mixture was fixed at 1 ppm. The pressure inside the reactor was kept at atmospheric pressure and measured *via* a MKS Baratron 622B capacitance manometer. Humidity of the inlet gas mixture was also carefully controlled by dosing varying amounts of water vapor into the inlet gas mixture (*i.e.* before the reactor entrance) with the help of a Perm Select (PDMSXA-2500) semi permeable membrane module attached to an external variable-temperature water chiller/recycler for controlling equilibrium vapor pressure of externally recycled water. Typical relative humidity (RH) of the reactor was kept within 50 ± 3% at 23 ± 2 °C, measured inside the reactor at the sample position using a Hanna HI 9565 humidity analyzer. Changes in the NO, NO_2, and total NO_x gas concentrations at the outlet of the reactor were monitored using a chemiluminescent NO_x analyzer, Horiba Apna-370

with a 0.1 ppb (*i.e.* 1×10^{-4} ppm) sensitivity and a data acquisition rate of 1 Hz.

For the experiments performed with UVA illumination, an 8 W UVA lamp (F8 W/T5/BL350, Sylvania, Germany) was utilized. The incoming light flux was measured carefully before and after each photocatalytic activity test with a photo-radiometer (HD2302.0, Delta Ohm/Italy) using a PAR UVA probe (315–400 nm). Typical UVA-light photon flux used in the current experiments was within 7.7–8.2 W/m^2, where reactor temperature remained within 23 ± 2 °C during photocatalytic measurements under UVA illumination. In each performance analysis test, 900 mg of photocatalyst was packed in a 2 mm × 40 mm × 40 mm poly methyl methacrylate (PMMA) sample holder and placed into the flow reactor. In this work, photocatalytic performance tests for each photocatalyst sample was performed at least three times and average values are reported. Deviation between independent performance measurements for a given photocatalyst was typically < 2%.

In order to quantify the photocatalytic activity and selectivity, three different performance parameters (*i.e.* % NO Conversion, % Selectivity towards NO_x Storage and $DeNO_x$ index) were obtained by integrating the concentration *versus* time plots, one of which is given as an example in Fig. 2. "*% **NO Conversion***" shows the total oxidation activity of the photocatalyst and its definition is given in equation (1). Therefore; achieving high NO conversion values is one of the desirable outcomes of PHONOS processes.

$$\%\,\textbf{NO Conversion} = \frac{\int ([NO]_{in} - [NO]_{out})dt}{\int [NO]_{in}dt} x\,100 \quad (1)$$

"% ***Selectivity***" is defined in equation (2). This term represents the percent of NO photo-oxidation products stored on the surface of the catalyst in solid state. Therefore; achieving high values of % Selectivity is essential.

$$\%\,\textbf{Selectivity}\ (\textit{towards}\ NO_x\ \textit{Storage}) = \frac{\int ([NO_x]_{in} - [NO_x]_{out})dt}{\int ([NO]_{in} - [NO]_{out})dt} x\,100 \quad (2)$$

These calculations assume that NO (g) conversion is only due to solid state NO_x storage and gaseous NO_2 generation, excluding the formation of other gaseous N-containing species such as N_2O (g) or N_2 (g). This is a reasonable assumption as the major products of the photocatalytic NO + O_2 reaction are NO_2 (g), HONO (ads), $HONO_2$ (ads) and NO_3^- (ads)/NO_2^- (ads) [43].

As mentioned earlier, NO_2 is much more toxic than NO. According to Occupational Safety and Health Administration (OSHA), American Conference of Governmental Industrial Hygienists (ACGIH) and National Institute for Occupational Safety and Health (NIOSH); short term exposure limit value of NO is 25 ppm while the corresponding limit value of NO_2 varies from 1 to 3 ppm [44]. The photolysis of NO_2 followed by its reaction with O_2 may also result in ozone (O_3) formation, which is even more toxic than other NO_x species with a limit value of 0.1 ppm [44]. Therefore, Bloh et al. proposed the $DeNO_x$ index parameter as a unique figure of merit in order to quantify the net NO_x abatement effect of a photocatalyst by both taking NO Conversion as well as NO_2 formation into account [17]. Their main assumption was that NO_2 contributes three times more than NO to the total toxicity of atmospheric NO_x. Based on these facts; while a preferable photocatalyst reveals a positive $DeNO_x$ index and has a net NO_x purification effect; a photocatalyst with a negative $DeNO_x$ index value has an overall toxification effect and thus not preferred. The parameter defined in equation (3) and used in the current work is a modified version of the $DeNO_x$ index proposed by Bloh and co-workers.

$$\textbf{De}NO_x\ \textbf{index} = \frac{\int ([NO]_{in} - [NO]_{out})dt - 3\int ([NO_2]_{out} - [NO_2]_{in})dt}{\int [NO]_{in}dt} \quad (3)$$

It should be noted that *% NO Conversion* and *% Selectivity* values defined above for a particular photocatalyst are not universally constant for a given gas composition, temperature and total gas mixture flow rate, but also vary with the incoming UVA photon flux. Hence, photocatalytic activity data can also be reported after normalization with the incident photon flux and calculation of the *% Photonic Efficiency* values as given in Eq.s (4) and (5) [45];

$$NO_x\ \textit{Storage \% Photonic Efficiency}\ (\xi) = \frac{n(NO_x\ \textit{stored on the catalyst surface})}{n(\textit{photon})} x\,100 \quad (4)$$

$$NO_2\ \textit{Release \% Photonic Efficiency}\ (\xi) = \frac{n(NO_2\ \textit{released to the atmosphere})}{n(\textit{photon})} x\,100 \quad (5)$$

where *n(photon)* is defined as:

$$n(\textit{photon}) = \frac{(I\,x\,\lambda\,x\,A\,x\,t)}{(N_A\,x\,h\,x\,c)} \quad (6)$$

In equation (6), "*I*" represents the photon power density of the lamp; λ represents the mean emission wavelength of the lamp; "*A*" is the surface area of the photocatalyst exposed to light irradiation; "*t*" represents the duration of the performance test; "N_A" is the Avogadro's number; "*h*" is the Plank constant and "*c*" is the speed of light.

Photonic efficiency % values described in Eqs. (4) and (5) denote the percentile of the number of NO_x species stored in solid state (or NO_2 (g) molecules released to gas phase) per number of photons impinging on the catalyst surface during a 60 min-long photocatalytic activity test. Since the ultimate goal of the current work is to determine/compare/quantify the actual amounts of NO_x abatement under irradiation conditions similar to that of solar radiation, we will mostly focus on the % NO Conversion and % Selectivity towards NO_x storage values in our discussion, however all representative photonic efficiency data are also provided in the Supporting Information Section (**Figs. S2-S6**).

3. Results and discussion

3.1. Structure analysis

Individual X-ray diffraction patterns of bare Degussa P25, γ-Al_2O_3 and CaO along with binary and ternary oxide systems are presented in Fig. 1. It can be seen in Fig. 1 that P25 reveals diffraction signals associated with predominantly anatase (ICDD Card no: 00-021-1272) and to a lesser extent, rutile (ICDD Card No: 00-021-1276) phases of titania. XRD pattern obtained for alumina (Fig. 1) shows characteristic

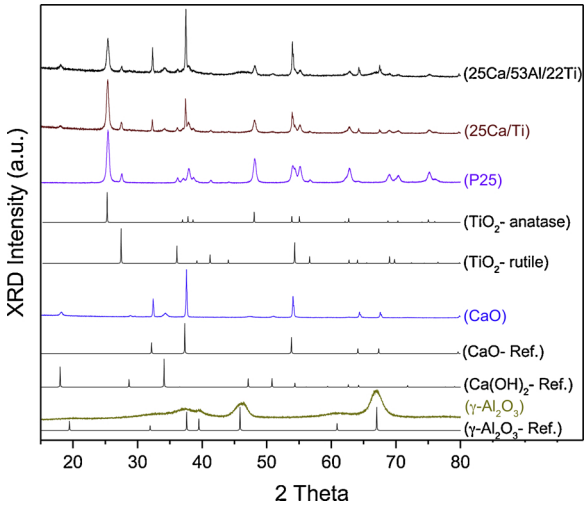

Fig. 1. XRD patterns of 25Ca/53Al/22Ti, 25Ca/Ti, Degussa P25, CaO and γ-Al_2O_3 materials used in the current study.

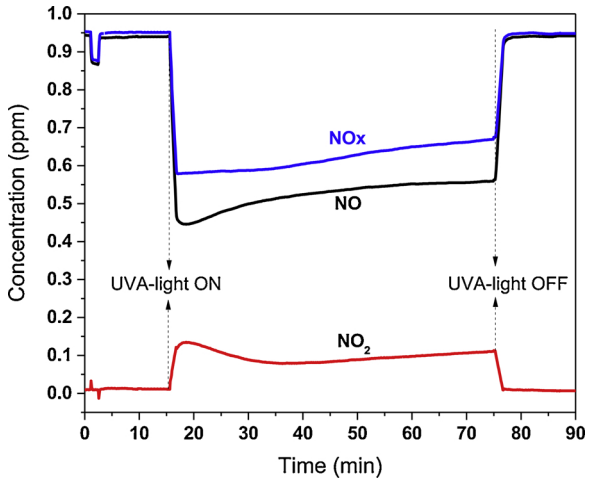

Fig. 2. Concentration *versus* time profiles obtained during a typical 1 h Photocatalytic NO_x(g) Oxidation and Storage (PHONOS) activity test performed on 25Ca/53Al/22Ti photocatalyst in a custom-made photocatalytic flow reactor. Red (bottom), black (middle) and blue (top) traces correspond to NO_2 (g), NO (g) and total NO_x (*i.e.* NO + NO_2) concentrations measured as a function of time (with a 1 Hz acquisition rate) during the photocatalytic activity test, respectively. Feed composition: N_2 (g) 0.750 SLM, O_2 (g) 0.250 SLM, and NO (g) 0.010 SLM (100 ppm NO (g) diluted in balance N_2 (g), RH 50% at 23 °C. (For interpretation of the references to colour in this figure legend, the reader is referred to the web version of this article).

diffraction features consistent with the γ-Al_2O_3 phase (ICDD Card No: 00-010-0425) [46]. On the other hand, XRD pattern of commercial CaO given in Fig. 1 is more complex due to the presence of CaO (ICDD Card No: 00-037-1497) and $Ca(OH)_2$ (ICDD Card No: 00-044-1481) phases. Calcium hydroxide is formed as a result of spontaneous reaction of CaO with atmospheric moisture [47].

SSA values of pure CaO, P25 and γ-Al_2O_3 used in the catalyst preparation were measured to be 3, 50, 200 m^2/g, respectively. Since the prepared binary and ternary mixed oxides were simple physical mixtures, SSA values of these materials can be readily determined using the weighted linear combination of the SSA values of their individual components. For instance, for a mixture with a particular composition of *x*Ca/*y*Al/*z*Ti (where, *x, y,* and *z* stand for the wt.% of each corresponding component), total SSA can be calculated as {(*x*(3) + *y*(200) + *z*(50))/100}. Validity of this expression was also experimentally verified using 25Ca/Ti sample (experimentally measured BET SSA = 39 m^2/g and SSA obtained by theoretical weighted linear combination = 38 m^2/g) and the 25Ca/53Al/22Ti sample (experimentally measured BET SSA = 113 m^2/g and theoretical SSA obtained by weighted linear combination = 118 m^2/g). *In-situ* FTIR spectroscopic experiments involving NO_2 adsorption (**Figs. S7a-S7c**) on CaO, TiO_2(P25) and γ-Al_2O_3 at room temperature revealed the formation of predominantly nitrate species and to a lesser extent to nitrite species with various adsorption geometries (*e.g.* monodentate, bidentate, bridging, *etc.*). NO_2-TPD experiments (**Figs. S7d-S7f**) indicated that among these three different materials, CaO yielded the highest NO_2 adsorption and storage capacity per unit catalyst mass, while TiO_2(P25) *and* γ-Al_2O_3 gave rise to a similar magnitude of NO_2 adsorption and storage capacity per mass of catalyst, which was lower than that of CaO (Fig. S8). Pyridine adsorption on CaO, TiO_2(P25) and γ-Al_2O_3 at room temperature was also investigated *via in-situ* FTIR spectroscopy which verified that the Lewis acidity of these materials increased in the following order: CaO < TiO_2(P25) < γ-Al_2O_3 (Fig. S9). In very good accordance with the current BET SSA measurements, SEM images (Figs **S10a-S10f**) suggest that average particle (grain) sizes of the CaO, TiO_2(P25) and γ-Al_2O_3 samples can be ranked in the following order: Al_2O_3 << TiO_2 << CaO. Furthermore, EDX analysis (Fig. **S10g-S10i**) also verified the chemical composition of these samples and indicated the lack of any contaminations. Furthermore, ex-situ FTIR experiments immediately performed after PHONOS activity tests (Fig. **S11**) verified the presence of nitrates on the spent photocatalysts.

3.2. Photocatalytic NO_x oxidation and storage (PHONOS) performance tests

In order to demonstrate the catalytic activity of the binary and ternary mixed oxide photocatalysts, we performed photocatalytic NO_x (g) oxidation and storage (PHONOS) tests using a custom-made photocatalytic flow reactor. UVA-light induced removal of NO (g) was monitored under *in-situ* conditions for different photocatalysts. Fig. 2 shows a typical set of time-dependent NO (g), NO_2 (g) and total NO_x (g) (*i.e.* NO (g) + NO_2 (g)) concentration profiles as a function of irradiation time during the NO photo-oxidation over 25Ca/53Al/22Ti photocatalyst. In the first stage of the photocatalytic activity tests, a synthetic polluted air gas mixture containing *ca.* 1 ppm NO (g) was fed to the photocatalyst surface under dark conditions. During this initial phase (*i.e.* first 15 min), a minor transitory fall in the total NO_x (g) and NO (g) concentrations was observed due to adsorption of NO_x species on the reactor lines, expansion of the gas in the reactor as well as non-photocatalytic adsorption of NO_x on the photocatalyst surface. In addition, a tiny amount of NO_2 (g) was produced due to thermal catalytic processes occurring on the catalyst surface. Following the saturation of the reactor system and photocatalyst surface, NO_x (g) and NO (g) levels quickly returned to the original inlet values and reached a steady state in dark conditions.

Next, UVA-light irradiation was turned on after the first *ca.* 15 min (Fig. 2) and a drastic fall in the NO (g) and total NO_x (g) concentrations was detected along with a small increase in the NO_2 (g) level. While the latter observation suggests the photocatalytic oxidation of NO (g) into NO_2 (g), decrease in the NO (g) and total NO_x (g) concentrations indicates the solid state storage of NO (g) and NO_2 (g) in the form of chemisorbed NO_2, nitrites and/or nitrates on the photocatalyst surface [5,48]. In principle, N_2 (g) and/or N_2O (g) can also be produced as a result of direct photocatalytic decomposition and photo-reduction of NO(g) [49]. However, this is known to be a relatively inefficient reaction pathway, particularly in the presence of O_2 and H_2O. Thus, N_2 and/or N_2O formation can readily be ruled out in the current study as insignificant photocatalytic routes [9]. It is apparent in Fig. 2 that photocatalytic NO_x abatement action continues after this initial stage during the entire duration of the activity test. Thus, total NO_x abatement effect can be calculated by integrating the relevant traces for the entire duration of the PHONOS test.

3.2.1. Enhancement of TiO_2 via incorporation of a basic oxide with a low specific surface area: PHONOS tests for CaO/P25 binary metal oxide mixtures

Photocatalytic NO_x (g) oxidation and storage (PHONOS) activity tests were performed for CaO/P25 binary oxides with different compositions and compared with that of a commercial benchmark P25 titania photocatalyst under identical experimental conditions (Fig. 3). Fig. 3**a** illustrates the NO (g) conversion % and NO_x storage selectivity % values. Meanwhile, overall photocatalytic NO_x abatement performances of all of the investigated photocatalysts are presented in Fig. 3**b** in terms of their corresponding $DeNO_x$ index values.

It is clear from Fig. 3a and b that P25 commercial benchmark has a reasonably high NO conversion. On the other hand, P25 benchmark catalyst also produces a very large quantity of unwanted NO_2 (g). Despite the fact that the adsorption capacity of TiO_2 for NO_2 (g) is much higher than that for NO (g) [50], photocatalytic NO_2 (g) production rate and the total number of NO_2molecules generated can readily overwhelm the NO_x adsorption capacity of titania leading to unwanted NO_2 slip/release into the atmosphere. Since NO_2 is a much more toxic pollutant than NO, P25 does not qualify as an efficient photocatalyst for NO_x abatement under UVA light irradiation, evident by its low NO_2

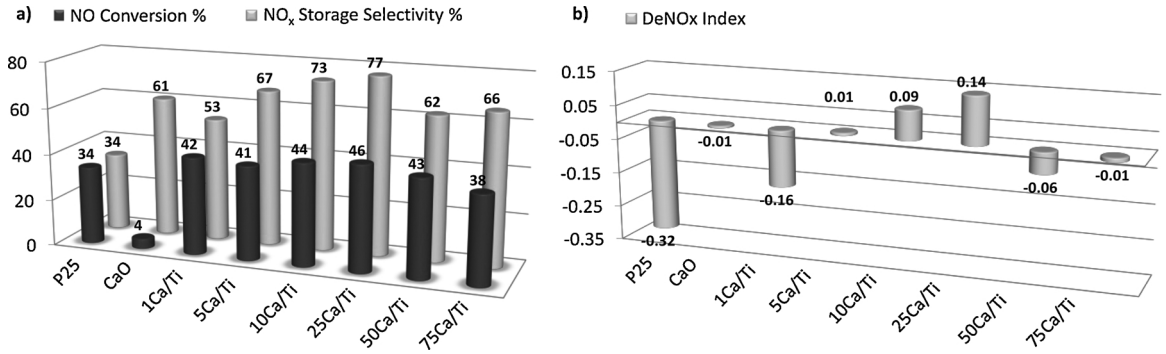

Fig. 3. NO (g) conversion %, NO_x storage selectivity % and $DeNO_x$ index values for different *CaO/P25 binary oxide-based* photocatalysts obtained under UVA-light irradiation.

storage selectivity and extremely negative $DeNO_x$ index (-0.32).

When the photocatalytic performances of CaO/P25 binary metal oxide-based photocatalysts are compared to that of P25 (Fig. 3), it can be seen that incorporation of CaO to P25 results in striking improvements such as increased NO conversion %, increased NO_x storage selectivity % (Fig. 3a), and increased $DeNO_x$ index values (Fig. 3b). Considering the relatively low surface area of the CaO material used in the current work (*i.e.* 3 m^2/g), significant boost in the observed NO_x storage for the CaO/P25 binary metal oxide-based photocatalysts suggests that the basic nature of the CaO is the main driving force for the enhanced NO_x storage selectivity.

Comparison of the relative photocatalytic performances of CaO/P25 binary oxides with different CaO loadings (Fig. 3b) clearly reveals a volcano-plot like behavior suggesting that 25Ca/Ti photocatalyst demonstrates the optimum performance by maximizing photocatalytic NO_x oxidation and storage, while minimizing the NO_2 release to the atmosphere. As opposed to P25 titania commercial benchmark photocatalyst, NO conversion % was improved from 34% to 46% and NO_x storage selectivity % was enhanced from 34% to 77% for 25Ca/Ti (Fig. 3a).

Here, it could be interesting to discuss the *ca.* 12% increase in NO conversion upon incorporation of a photocatalytically inactive component such as CaO to P25 (Fig. 3). This can be partly explained by non-photocatalytic (passive) NO adsorption and storage on CaO, as Fig. 3 shows that pure CaO can lead to *ca.* 4% NO conversion. The boost in NO conversion after diluting P25 with CaO can be explained by considering a synergistic interaction between titania (P25) photocatalytic active sites and CaO non-photocatalytic storage sites, where the surface and gas phase transport/diffusion of NO_x oxidation products from the active sites of titania (P25) towards the CaO domains prevents the saturation/poisoning of the titania active sites with the reaction products. This can be supported *via* the photocatalytic mechanism proposed by Macphee et al. (reactions 7–17) [41]. When NO_2 is transported from the titania surface to the calcium oxide surface in vicinity; radicals used in NO_2 oxidation reactions (16,17) become available to be utilized in NO oxidation reactions (10,14,15) rather than in NO_2 oxidation. Hence, the increase in the availability of reactive species eventually leads to an increase in total NO conversion in the CaO/P25 system.

$$TiO_2 + h\nu \rightarrow TiO_2(h^+ + e^-) \quad (7)$$

$$TiO_2(h^+) + H_2O_{ads} \rightarrow TiO_2 + {}^{\bullet}OH_{ads} + H^+ \quad (8)$$

$$TiO_2(e^-) + O_{2ads} \rightarrow TiO_2 + O_2^{\bullet-}ads \quad (9)$$

$$NO_{ads} \xrightarrow{{}^{\bullet}OH_{ads}} HNO_{2ads} \xrightarrow{{}^{\bullet}OH_{ads}} NO_{2ads} + H_2O \quad (10)$$

$$NO_{ads} \xrightarrow[H^+]{O_2^{\bullet-}{}_{ads}} NO_{2ads} + {}^{\bullet}OH \quad (11)$$

$$NO_{ads} \xrightarrow[H^+]{O_2^{\bullet-}{}_{ads}} HNO_{3ads} \quad (12)$$

$$TiO_2(h^+) + TiO_2(O_S) \rightarrow TiO_2(O_S^{\bullet}) \quad (13)$$

$$NO_{ads} \xrightarrow[H_2O]{TiO_2(O_S^{\bullet})} TiO_2 + NO_{2ads} + 2H^+ \quad (14)$$

$$NO_{ads} \xrightarrow{TiO_2(O_S^{\bullet})} NO_{2ads} + TiO_2(V) \xrightarrow{H_2O} TiO_2 + 2H^+ \quad (15)$$

$$NO_{2ads} + {}^{\bullet}OH_{ads} \rightarrow HNO_{3ads} \quad (16)$$

$$NO_{2ads} \xrightarrow[H_2O]{TiO_2(O_S^{\bullet})} TiO_2 + {NO_3}^-{}_{ads} + 2H^+ \quad (17)$$

Furthermore, the findings of Rodriguez and co-workers [51] about nitrate formation on TiO_2 (110) rutile surface can also enlighten the better performance of binary mixtures. In their study, it was reported that surface nitrate formation occurs *via* the disproportionation of NO_2 on Ti sites (reaction 18) rather than the direct NO_2 adsorption on O sites. Due to this disproportion mechanism, produced NO molecules decrease the total conversion of NO. Thus, when NO_2 molecules are transferred to non-photocatalytic NO_x storage domains of the binary mixture, NO_2 disproportion rate on Ti sites diminishes which in turn, boosts the NO conversion on titania.

$$2NO_{2ads} \rightarrow {NO_3}^-{}_{ads} + NO^+_{ads} \quad (18)$$

It is also interesting to note that photocatalytic performance of CaO/P25 binary oxides start to deteriorate once CaO loading exceeds 25 wt.%. This is probably due to the fact that for CaO loadings higher than 25 wt.%: *i)* number of photocatalytically active titania sites present in the catalyst formulation decreases below a critical value along with the decreasing relative loading of titania in the binary mixture, *ii)* CaO grains start to physically cover P25 active sites and prevent their access to both incoming UVA irradiation and inlet reactant flow (through mass transfer limitations).

These photocatalytic results suggest that the primary photocatalytic active sites of the CaO/P25 system that are responsible for the NO (g) photooxidation process reside on titania, since addition of different CaO loadings led to only a minor boost in NO conversion. However, a synergistic effect between CaO and titania (moderately increasing the NO conversion capability) cannot be ruled out under UVA irradiation. On the other hand, while CaO seem to increase NO conversion to a certain extent, the more noteworthy function of CaO is the storage of photogenerated NO_2 species into other oxidized surface species. It is well known that NO (g) + O_2 (g) mixtures as well as NO_2 (g) can readily adsorb on numerous metal oxide surfaces in the form of nitrates, nitrites, as well as their protonated acidic forms [24,26,27,30,39,40,52]. NO_x adsorption and successive oxidation and storage in the form of nitrates also serve as the basis of the non-photocatalytic NSR catalysis (also called lean NO_x traps, LNT) that is commonly used in tail-pipe emission control systems of automobiles [5–7].

To be an effective photocatalyst, the conversion of the toxic NO_2 to ${NO_3}^-$ needs to be more efficient than the conversion of NO to NO_2.

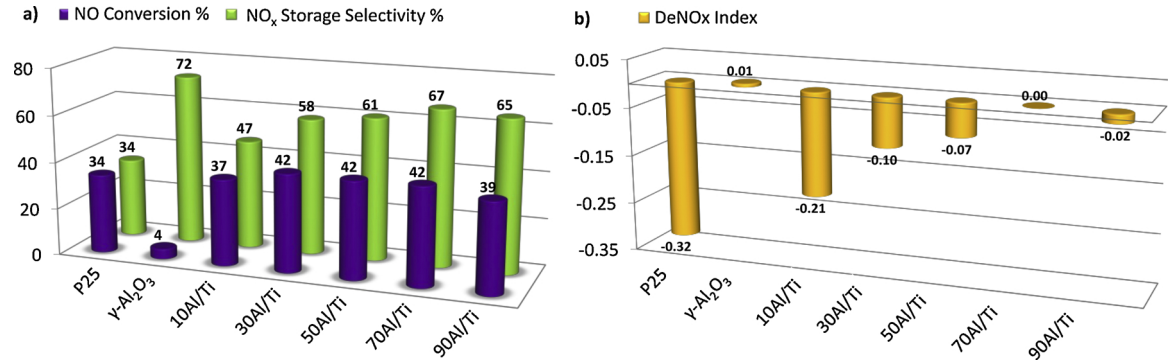

Fig. 4. NO (g) conversion %, NO_x storage selectivity % and $DeNO_x$ index values for different γ-*Al_2O_3/P25 binary oxide-based* photocatalysts obtained *via* UVA-light irradiation.

Such a catalyst would demonstrate a high selectivity towards nitrate formation and can have a significant positive effect on the resulting air quality. Fig. 3**b** indicates that CaO incorporation to titania improves both NO conversion and NO_2 storage selectivity, leading to a high and a positive $DeNO_x$ index value for 25Ca/Ti (+0.14, Fig. 3b) which significantly surpasses that of P25 titania commercial benchmark photocatalyst with a $DeNO_x$ index value of -0.32. In other words, while P25 titania commercial benchmark photocatalyst does not reveal a net NO_x abatement effect under UVA irradiation, 25Ca/Ti photocatalyst shows a strong overall photocatalytic detoxification action under UVA irradiation.

3.2.2. *Enhancement of TiO_2 via incorporation of an acidic oxide with a high specific surface area: PHONOS tests for γ-Al_2O_3/P25 binary metal oxide mixtures*

Next, γ-Al_2O_3/P25 binary oxides with varying compositions were tested for NO_x abatement under UVA irradiation. The corresponding conversion and selectivity values for γ-Al_2O_3/P25 binary oxides are shown in Fig. 4. Fig. 4a indicates that addition of γ-Al_2O_3 to P25 improves the NO_x storage capacity in a noticeable manner, while enhancing the NO conversion rather marginally. The optimum performance among the investigated γ-Al_2O_3/P25 binary oxides was achieved for the 70Al/Ti sample. It must be noted here that the maximum NO_2 storage selectivity of 67% achieved by the best performing γ-Al_2O_3/P25 binary oxide (*i.e.* 70Al/Ti) was still lower than that of the best CaO/P25 photocatalyst (*i.e.* 25Ca/Ti with a selectivity of 77%). This shows that in the case of binary mixed oxides, greater basicity of CaO in CaO/P25 samples is a more decisive factor than the higher surface area of γ-Al_2O_3 in the γ-Al_2O_3/P25 binary mixtures (note that SSA values of 25Ca/Ti *vs.* 70Al/Ti are 39 m^2/g *and* 155 m^2/g, respectively).

$DeNO_x$ Index values for γ-Al_2O_3/P25 photocatalysts given in Fig. 4**b** show that 70Al/Ti reveals the best performance among all of the investigated γ-Al_2O_3/P25 binary mixtures under UVA irradiation. It is imperative to mention here that although 70Al/Ti is the γ-Al_2O_3/P25 binary mixture with the highest $DeNO_x$ index value of *ca.* 0.001 (shown as 0.00 in Fig. 4b), it is still well below the $DeNO_x$ index value of 25Ca/Ti (+0.14). Although the SSA of 70Al/Ti is significantly higher than that of 25Ca/Ti (*i.e.* 155 m^2/g *vs* 39 m^2/g, respectively), lower performance of 70Al/Ti indicates that rather than the SSA, surface basicity of the NO_x storage domain is the determining factor for the ultimate performance of the P25 titania systems modified with additional metal oxides for NO_x storage. This observation also indicates that although number of available surface adsorption sites per gram of material is much greater for γ-Al_2O_3 than that of CaO, because of the relatively weaker adsorption energy of NO_2 species on γ-Al_2O_3, as compared to that of CaO, γ-Al_2O_3 can store a significantly smaller number of NO_2 molecules on its surface.

Here, it is also worth mentioning that in order to assess the photocatalytic performance properly, $DeNO_x$ index values (Fig. 4b) should also be evaluated along with the corresponding NO Conversion % and NO_2 Storage Selectivity % values (Fig. 4a). To illustrate this, one may consider the $DeNO_x$ index value of pure γ-Al_2O_3 which is higher than that of any of the other γ-Al_2O_3/P25 photocatalyst, as well as pure P25 benchmark photocatalyst (Fig. 4b). Careful investigation of Fig. 4**a** clearly yields that γ-Al_2O_3 is almost entirely inactive (*i.e.* NO Conversion 4%) and hence, yields a $DeNO_x$ value of *ca.* 0.01 due to the lack of any notable activity. In contrast, 70Al/Ti has a significantly high photocatalytic activity, however high NO conversion of 70Al/Ti is accompanied by low NO_2 storage selectivity, rendering it a photocatalyst with a $DeNO_x$ index value of *ca.* 0.001 (shown as 0.00 in Fig. 4b).

3.2.3. *Enhancement of TiO_2 via incorporation of both a basic and an acidic oxide: PHONOS tests for CaO/γ-Al_2O_3/P25 ternary metal oxide mixtures*

As discussed above, best photocatalytic $DeNO_x$ performance among the γ-Al_2O_3/P25 catalysts was achieved for the 70Al/Ti sample (Fig. 4b). Therefore, this catalyst was further enriched with CaO in an attempt to further improve its performance and also to obtain a more affordable photocatalyst formulation for large scale applications by decreasing the relatively more expensive titania content. PHONOS test results for these ternary metal oxide mixtures (CaO/γ-Al_2O_3/P25) are given in Fig. 5. Based on these results, it was found that among the analyzed CaO/γ-Al_2O_3/P25 ternary mixed oxides, the highest $DeNO_x$ index value of + 0.27 was obtained for the 50Ca/35Al/15Ti sample, which was even higher than that of 25Ca/Ti binary mixed oxide sample (+0.14) (Fig. 3). These observations reveal a delicate trade-off between the relative basicity and the relative SSA of the NO_x storage domains. It is apparent that increasing the overall basicity of the metal oxide mixture by increasing the corresponding CaO content/loading, increases the number of strongly binding NO_x adsorption sites. However, this positive effect is obtained at the expense of the decreasing SSA and porosity of the overall mixture, which hinders NO_x transport from the gas phase to the surface. Therefore, it is clear that in the case of a ternary metal oxide mixture with an optimized formulation (*e.g.* 50Ca/35Al/15Ti), photocatalytic system can utilize both the strongly-binding adsorption sites of the basic CaO as well as the weakly/moderately-binding adsorption sites of the more acidic γ-Al_2O_3 domains, without sacrificing the total surface area of the mixture. Furthermore, although the total number of photocatalytic active sites (*i.e.* TiO_2 loading) in 50Ca/35Al/15Ti is less than that of P25, 25Ca/Ti and 70Al/Ti samples, they are still sufficient to provide a superior performance in the first 1 h of the PHONOS tests.

However as will be demonstrated in the next section, this initially superior performance of the 50Ca/35Al/15Ti system containing only 15 wt.% TiO_2 may quickly deteriorate during the operation of the catalyst for extended durations of time, due to the saturation/blocking/poisoning of the photocatalytic active sites on TiO_2 with NO_x oxidation products, emphasizing the importance of the TiO_2 loading in the overall ternary mixed oxide formulation.

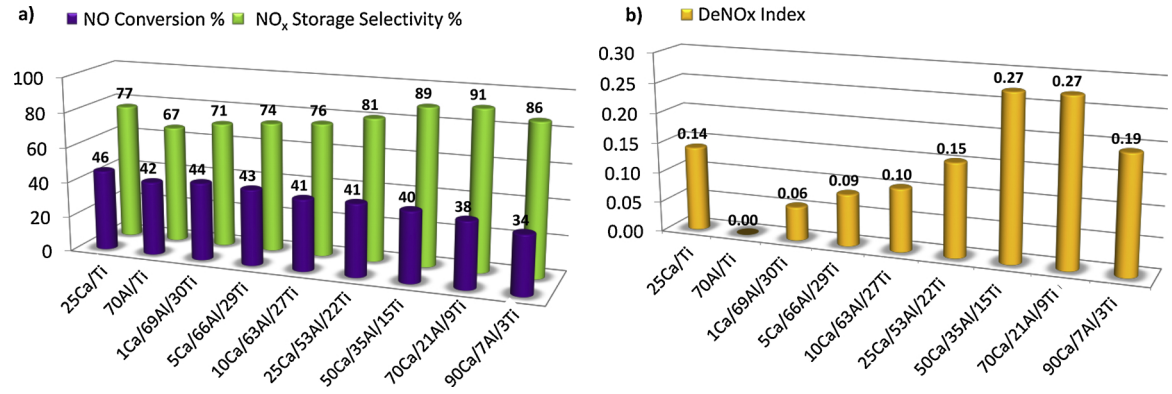

Fig. 5. NO (g) conversion %, NO_x storage selectivity % and $DeNO_x$ index values for different *CaO/γ-Al_2O_3/P25 ternary oxide-based* photocatalysts obtained *via* UVA-light irradiation.

3.2.4. *Long-term performance and catalytic stability tests*

Long-term photocatalytic stability is an essential requirement for end user applications. Thus, in order to demonstrate the photocatalytic stability of the currently investigated materials, we performed a series of long-term PHONOS experiments under continuous UVA irradiation. When the corresponding data for pure P25 in Fig. 6**a** is examined, it can be immediately noticed that NO conversion % of P25 stays almost invariant during the entire 12 h stability test with only a minor attenuation of 2%. On the other hand, NO_x storage selectivity of P25 monotonically decreases over time due to the saturation of the P25 surface with photo-oxidation products. It can be seen in Fig. 6**a** that NO_x storage selectivity of P25 decreases from 34% to 23% (*i.e.* decreases to 0.3 times of its original value) after the 12 h stability test. This loss in selectivity is also apparent by the monotonically decreasing $DeNO_x$ index value of the P25 commercial benchmark catalyst measured during the 12 h stability test **(**Fig. 6b**),** rendering the spent P25 catalyst an extremely unpreferable photocatalyst with a severely negative $DeNO_x$ index value of -0.37. Therefore, it can be argued that the loss in overall photocatalytic performance of P25 commercial benchmark photocatalyst upon extended duration of use is mostly due to the loss in NO_x storage selectivity and to a lesser extent due to the loss in NO conversion.

Fig. 6**a and b** show that NO conversion %, NO_x storage selectivity %, and $DeNO_x$ index values decrease monotonically in a drastic fashion as a function of time for the 70Al/Ti and 50Ca/35Al/15Ti samples. During the 12 h stability test, $DeNO_x$ index value of 70Al/Ti falls from 0.00 to -0.13, while $DeNO_x$ index value of 50Ca/35Al/15Ti decreases from +0.27 to +0.05.

It is important to note that as in the case of P25, decrease in NO conversion % is also relatively minor for the 70Al/Ti catalyst, suggesting that both P25 and 70Al/Ti catalysts still exhibit a sufficiently large number of available photocatalytically active sites even after 12 h of operation and they mostly suffer from the loss in NO_x storage selectivity due to the adsorption of oxidation products on the acidic γ-Al_2O_3 domains (*i.e.* saturation of alumina).

On the other hand, this is not the case for the 50Ca/35Al/15Ti ternary mixed oxide photocatalyst, where concomitant to NO_x storage selectivity, NO conversion also shows a very substantial decrease after 12 h of operation. This can be attributed to the scarcity of the titania active sites in the 50Ca/35Al/15Ti catalyst composition (note that TiO_2 wt.% in the 25Ca/Ti, 70Al/Ti and 50Ca/35Al/15Ti catalysts are 75, 30, and 15 wt.%, respectively). These limited number of titania active sites are blocked by the oxidation products upon extended durations of operation, leaving an insufficiently small number of titania active sites for photocatalytic oxidation.

Interestingly, photocatalytic stability data for 25Ca/Ti given in Fig. 6**a and b** show that in spite of the measurable decrease in NO conversion %, 25Ca/Ti is capable of preserving most of its NO_x storage selectivity over time. Along these lines, $DeNO_x$ index value of 25Ca/Ti (+0.14) obtained after the first 1 h of the stability test, decreases to a value of +0.09 after the 12 h stability test. In other words, 25Ca/Ti exhibits an efficient detoxification (NO_x abatement) function even after 12 h of use, outperforming P25 titania commercial benchmark and 70Al/Ti catalysts (which remain unacceptable $DeNO_x$ photocatalysts during the entire photocatalytic stability tests), or the 50Ca/35Al/15Ti photocatalyst (which quickly loses its initially favorable performance after 12 h).

It should be highlighted that although the total duration of the stability tests presented in Fig. 6 was 12 h, these tests can reflect even much longer-term performances of the investigated catalysts that may presumably extent to many days. This is due to the fact that all of the current PHONOS performance tests were carried out using a NO(g) concentration of 1 ppm (or 1000 ppb). On the other hand, typical NO (g) pollution levels in urban settings (Table S1**)** are typically 10 to 20

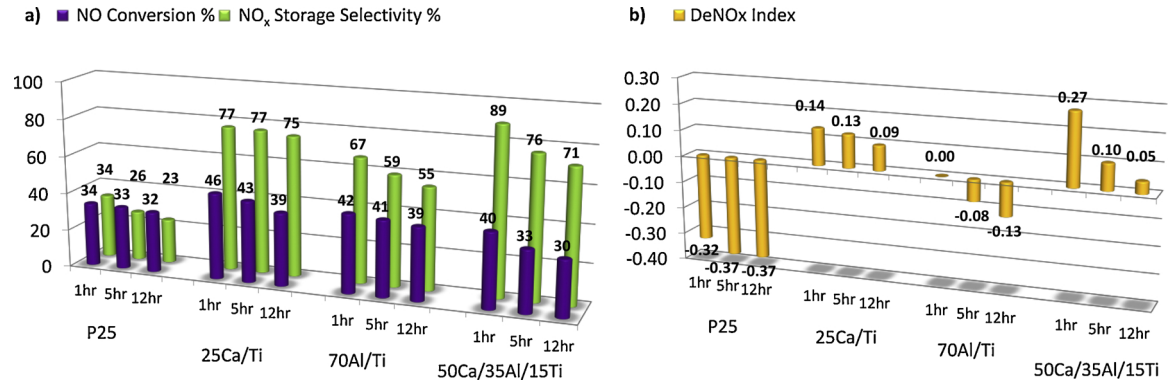

Fig. 6. NO (g) conversion %, NO_x storage selectivity % and DeNOx index values of selected samples during long term stability tests carried out under UV irradiation.

times less than the currently used NO (g) concentration of 1000 ppb. Therefore, currently studied photocatalysts are likely to preserve their catalytic performances under realistic urban settings for durations that are much longer than the duration of the currently performed 12 h stability tests. From this perspective, currently presented stability tests can be considered as accelerated performance tests.

This argument is also supported by the work of Yu et al. [53], demonstrating that the inlet concentration of NO_x plays an important role in the photocatalytic activity of semiconductors. In their study, they conducted photocatalytic NO oxidation using NO concentrations ranging from 0.1 ppm to 1.0 ppm while keeping other experimental parameters constant. They reported that NO conversion decreased with increasing NO concentration. This finding was later confirmed by Husken and co-workers [54], who verified that higher pollutant concentrations diminished the $DeNO_x$ performance. Therefore, it is clear that the photocatalytic performance results presented in the current work at high NO_x concentrations can be considered as "lower-bound" values and the operational performance of the currently investigated photocatalytic materials under realistic (*i.e.* lower) urban atmospheric NO_x levels are expected to be greater than the currently reported values. Accordingly, materials studied here are likely to operate effectively over a duration of many days under realistic urban NO_x pollution levels.

3.2.5. Effect of humidity on PHONOS performance

Interaction of water with catalytic metal and metal oxide surfaces have been summarized in two extremely comprehensive reviews by first Thiel and Madey [55] and later by Henderson [56]. These reviews as well as other more recent studies [41,57] provide a vast number of examples where adsorbed molecular water and/or the dissociation products of adsorbed water (*e.g.,* protons, hydroxyl radicals or hydroxide species) can either facilitate or hinder catalytic reactivity under different conditions. As can be seen in reactions (7–17) given above [41], photon absorption and electron-hole ($e^- - h^+$) pair generation on titania surface (reaction 7) results in the appearance of two separate branches of photocatalytic $DeNO_x$ pathways which include either hole-mediated or electron-mediated steps. Hole-mediated routes are either initiated by the dissociation of adsorbed molecular water (reaction 8) forming $\bullet OH_{ads}$, and H^+ species or trapping of holes by surface oxygen species of titania as in reaction 13. On the other hand, electron-mediated pathways begin with the adsorption of O_2 on titania and formation of superoxide ($O_2^{-}\bullet$) species (reaction 9). Hence, it was reported that both molecularly adsorbed (chemisorbed/physisorbed) water as well as dissociated water species are essential to initiate photocatalytic $DeNO_x$ pathways [41].

Having said that, in a recent related study, it was shown by Wang et al. [58] that during the hole-mediated photocatalytic decomposition of trimethyl acetate, photocatalytic activity was hindered by water due to the dissociation of water on oxygen vacancies of titania, forming bridging OH (OH_b) surface species which act as electron traps and form charged hydroxyl (*i.e.* hydroxide) species. It was shown by these authors that charged OH_b hydroxide surface functionalities serve as hole scavengers, facilitating electron-hole recombination and eventually, diminish the photocatalytic oxidation performance of titania. In the case of photocatalytic NO_x oxidation and storage (PHONOS), nitrogen atoms in NO (g) possess an oxidation state of +2 and are photocatalytically oxidized to +3, +4, or +5 states and form NO_2^-, NO_2, and NO_3^- (as well as protonated forms of some of these species) [39]. In other words, being an oxidation reaction, PHONOS reaction mechanism has a strong dependence on the hole concentration on the titania surface which drive the hole-mediated photocatalytic $DeNO_x$ pathways initiated by reaction 8. Hence, generation of hole scavengers such as negatively charged surface hydroxide species may hinder the photocatalytic activity by facilitating $e- h^+$ recombination at the surface hydroxide sites.

In addition, presence of excess concentrations of water at high RH may trigger disassociation of nitrites and/or nitrates into NO_2 through two different pathways. In the first pathway, interaction of physisorbed water molecules and NO_2 (reaction 19) leads to nitrate/nitrate dissociation in a non-photocatalytic manner to form NO, decreasing the total NO conversion [41,59]. The second pathway may include dimerization of HO• radicals. When the surface coverage of water increases, HO• radicals, which are essential for NO_x oxidation, can be consumed by forming hydrogen peroxide which decomposes into O_2 and H_2O (reaction 20,21). Therefore, the decrease in NO conversion becomes unavoidable [60].

$$3NO_2 + H_2O \rightarrow NO + 2HNO_3 \quad (19)$$

$$TiO_2\_OH^{\bullet} + TiO_2\_OH^{\bullet} \rightarrow TiO_2\_H_2O_2 \quad (20)$$

$$H_2O_2 \rightarrow H_2O + {}^{1}/_{2}O_2 \quad (21)$$

Here, it should be noted that humidity effects discussed above are subject to significant variations as a result of changes in experimental/operational conditions and reactor design. It has been reported that, when relatively lower NO concentrations (*e.g.* 1 ppm) were used to investigate the influence of relative humidity on conversion, rate of NO photo-oxidation decreased with increasing relative humidity (as observed in our current results, Fig. 7) [54,61]. On the other hand, when higher NO concentrations were used (*e.g.* 5–147 ppm), NO conversion either increased or remained invariant with increasing relative humidity (RH) [62–64]. Furthermore, for relatively lower initial concentrations of NO such as ≤ 1 ppm, competition between NO and water for surface adsorption sites was reported to be a less critical phenomenon [53,65]. Consequently, conversion and storage performances of a photocatalytic material should be evaluated under comparable experimental conditions by considering the effects of critical parameters such as RH, flow rate, composition of the feed gas, experimental setup and design, catalyst loading, sample preparation techniques, type/power/emission spectrum of the irradiation light source, feed gas temperature

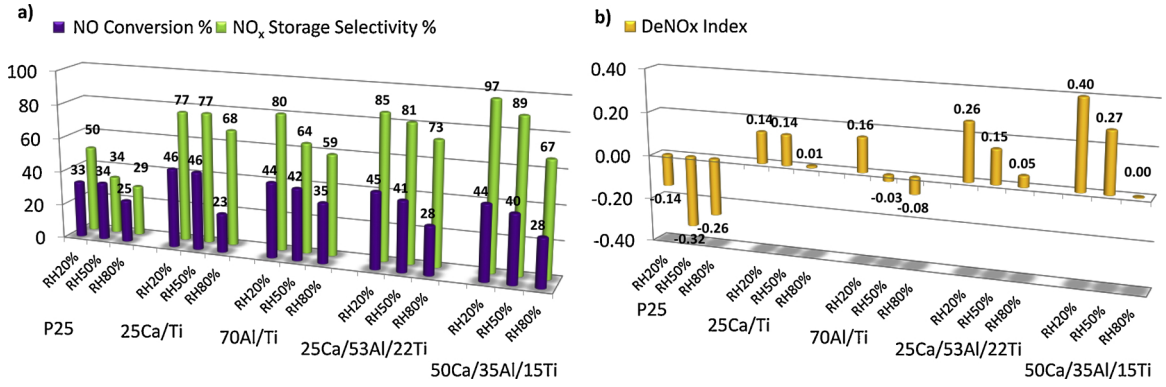

Fig. 7. NO (g) conversion %, NO_x storage selectivity % and $DeNO_x$ index values of selected samples during humidity tests carried out under UV irradiation.

and the catalyst surface temperature during the irradiation.

Therefore, the general reactivity trends in Fig. 7**a** for P25, 25Ca/Ti, 70Al/Ti, 25Ca/53Al/22Ti and 50Ca/35Al/15Ti suggest that at 20% RH, there is a sufficient number of adsorbed water molecules that can trigger photocatalytic hole-mediated reactions, resulting in high NO conversion, as well as high NO_2 storage selectivity. Furthermore, at 20% RH, surface concentration of adsorbed water species is not detrimentally high and most of the photocatalytic active sites on titania are still available for NO and NO_2 adsorption and further reaction.

When the RH% was increased to 50%, P25 benchmark catalyst exhibits a minor change in NO conversion but shows a drastic fall in its NO_2 storage selectivity (Fig. 7a**)**. This observation indicates that at 50% RH, P25 still possesses a sufficient number of exposed (unblocked) photocatalytic adsorption sites to perform efficient NO oxidation to NO_2. However, at 50% RH, generated NO_2 cannot be stored efficiently in the form of nitrates/nitrites possibly due to the increased surface concentration of charged OH_b (hydroxide) species acting as hole-scavengers as well as due to other non-catalytic suppression pathways discussed above. Finally, under extremely high humidity conditions (*i.e.* 80% RH), both NO conversion, and NO_2 storage selectivity values of P25 benchmark photocatalyst decrease in a drastic manner due to the increasing number of charged OH_b (hydroxide) hole-scavengers as well as increasing competitive adsorption of molecular water on titania photocatalytic active sites preventing the adsorption of reaction products such as NO and O_2. Along these lines, it can be seen in Fig. 7**b** that P25 benchmark catalyst exhibits severely negative $DeNO_x$ index values at all of the investigated humidity conditions, with a $DeNO_x$ index revealing its highest value at 20% RH.

In the case of 25Ca/Ti sample, Fig. 7**a** indicates that, both photocatalytic NO conversion and NO_2 storage selectivity are practically identical at 20 and 50% RH. This argument suggests that in the 25Ca/Ti binary mixture, due to presence of a large amount of titania (75 wt.%) in the catalyst composition, titania active sites are still not blocked in a severe fashion by the competitive adsorption of molecular water or its dissociation products at 20 and 50% RH. Within this humidity range, it is likely that basic CaO surface sites serve as a sacrificial adsorption sites that can capture water and prevent increasing surface coverages of competitively adsorbing water and hinder the formation of a large number of charged OH_b (hydroxide) hole-scavengers on titania sites.

On the other hand, when the RH value was increased to 80%, a drastic decrease in NO conversion along with only a mild decrease in NO_2 selectivity was observed for the 25Ca/Ti sample (Fig. 7a). It is apparent that at 80% RH, 25Ca/Ti system is still capable of storing photocatalytically generated NO_2 species in the form of nitrates/nitrites on the basic CaO domains, as well as on the hydrated forms of the CaO domains. In stark contrast, photocatalytic oxidation of NO to NO_2 on titania was severely suppressed indicating poisoning of the titania photocatalytic active sites. This observation can be explained in the light of the detailed surface spectroscopic (infrared reflection absorption spectroscopy, IRAS and X-ray photoelectron spectroscopy, XPS), surface imaging (scanning tunneling microscopy, STM) and density functional theory (DFT) computational modeling studies of Fujimori et al. [66] on the interaction of water with CaO(001) ultrathin films grown on Mo(001) substrate at room temperature. In this work, authors report that hydration of CaO(001) with water occurs in a gradual manner in several stages, where in the earlier stages (*i.e.* at relatively smaller water coverages of < 0.3 ML, ML: monolayer) small water/hydroxyl clusters aggregate on the CaO(001) surface. When the CaO (001) surface is saturated with water to obtain a surface water coverage of 0.5 ML, CaO(001) surface forms a fully hydroxylated and a heavily reconstructed (disordered) state exhibiting partially solvated Ca^{2+} and OH^- ions on its surface. Based on these findings, it can be argued that under extremely humid conditions, $DeNO_x$ performance of 25Ca/Ti photocatalyst (Fig. 7) deteriorates due to *i)* hydration of the CaO domains, *ii)* formation of solvated Ca^{2+} and OH^- species on the hydroxylated CaO domains, and *iii)* diffusion/transport of these species on titania domains, leading to site blocking by competitive adsorption on titania active sites, generation of hole-scavenging sites on titania, and occurrence of other non-photocatalytic hindering reactions (reactions 19–21).

In the case of 70Al/Ti binary mixture, PHONOS behavior at 20 and 50% RH values can be explained in an analogous manner to that of 25Ca/Ti, where, high surface area γ-Al_2O_3 domains act as sacrificial adsorption sites for water, preventing the poisoning of titania active sites at low and medium humidity conditions. On the other hand, it should be noted that γ-Al_2O_3 is a relatively acidic metal oxide exhibiting predominantly weaker NO_x adsorption sites, in addition to a much fewer number of moderate-strength NO_x adsorption sites. Therefore, NO_2 storage selectivity of γ-Al_2O_3 is much more susceptible to the loss of the moderately binding NO_x adsorption sites on γ-Al_2O_3 due to competitive water adsorption. It was reported in the literature that presence of high concentrations of water may decrease the nitrate formation on alumina by a factor of 90% due to the formation of hydroxyl groups on alumina [35,37]. This is also evident in the 80% RH data for 70Al/Ti (Fig. 7), where NO_2 selectivity reveals a significant attenuation at extreme humidity values. Interestingly, NO conversion on 70Al/Ti is not affected as severely as in the case of 25Ca/Ti. This is in stark contrast to the 25Ca/Ti system and can be attributed to the lack of the generation of solvated OH^- ions on γ-Al_2O_3 which are also not transferred onto titania domains to form hole-scavenging sites.

Influence of humidity on the 25Ca/53Al/22 Ti and 50Ca/35Al/15Ti samples reveal patterns that are in between that of 25Ca/Ti and 70/Ti binary mixtures, as can be expected from the composition of these ternary mixtures which bear combined traits of both of these different binary mixtures. At RH values of 20 and 50%, both 25Ca/53Al/22Ti and 50Ca/35Al/15Ti ternary mixtures can maintain significantly positive $DeNO_x$ index values, albeit a decrease in such values with increasing humidity (due the deactivation phenomena discussed above for P25 25Ca/Ti, and 70Al/Ti samples). On the other hand, upon exposure to extreme humidity, both 25Ca/53Al/22 Ti and 50Ca/35Al/15Ti ternary mixtures reveal a stark decrease in $DeNO_x$ index values. This observation suggests that the ternary oxide with a fewer number of titania active sites (*i.e.* mixture with the lower TiO_2 wt.%, 50Ca/35Al/15Ti) seems to be prone to a more severe performance loss.

In overall, currently presented humidity-dependent PHONOS tests on binary and ternary mixed oxide photocatalytic systems suggest that presence of low to moderate (20–50%) RH levels is crucial for the photocatalytic NO_x oxidation, while higher levels of RH (*e.g.* 80% RH) can be detrimental.

4. Conclusion

Major findings of the current work can be summarized as follows:

- 25 wt.% CaO addition to P25 titania significantly enhances both short term (1 h) as well as long term (12 h) PHONOS performance of P25, enabling CaO/P25 binary mixtures to significantly outperform conventional P25 titania benchmark photocatalysts. These positive effects were attributed to a synergistic interaction between titania and CaO domains boosting NO conversion as well as the extreme basicity of the CaO domains providing strong adsorption sites for NO_2 storage. An important shortcoming of the investigated CaO/P25 binary mixtures was identified to be their relatively low SSA values (*i.e.* 39 m^2/g).
- Although, 70 wt.% Al_2O_3 addition to P25 leads to noticeable improvement in both short term (1 h) and long term (12 h) PHONOS performance, as well as a drastic increase in SSA (*i.e.* 155 m^2/g), $DeNO_x$ index values of γ-Al_2O_3/P25 binary mixtures were not high enough to consider them as acceptable $DeNO_x$ photocatalysts. This was mostly attributed to the presence of weak/moderate strength NO_2 adsorption sites on γ-Al_2O_3.
- Hence, CaO/γ-Al_2O_3/P25 ternary mixtures were prepared

containing both highly-basic CaO domains for strong NO_2 adsorption, as well as more acidic γ-Al_2O_3 sites for low/medium strength NO_2 adsorption. Optimized ternary mixed oxide (25Ca/53Al/22/Ti) revealed a high SSA (*i.e.* 113 m^2/g) and a favorably positive $DeNO_x$ index after 1 h and 12 h PHONOS tests.

- PHONOS performance tests carried out at varying RH values of 20, 50 and 80% at 23 °C showed that $DeNO_x$ performance deteriorated with increasing RH. 25Ca/53Al/22/Ti preserved its favorable overall detoxification effect under all of the investigated RH conditions, while, 25Ca/Ti and 70Al/Ti binary mixtures lost their overall NO_x abatement capabilities at 80% RH.
- Using the mechanistic findings reported in the current text, ultimate composition of ternary mixtures can be fine-tuned in order to engineer photocatalytic systems with high initial performance, long-term stability and enhanced tolerance against extreme humidity.

Declaration of Competing Interest

The authors declare that they have no known competing financial interests or personal relationships that could have appeared to influence the work reported in this paper.

Acknowledgements

EO, MI, MC acknowledge the financial support from the Scientific and Technological Research Council of Turkey (TUBITAK) (Project Code: 116M435). Authors thank SASOL GmbH for providing PURALOX SBa200 γ-Al_2O_3 materials. EO acknowledges the scientific collaboration with TARLA project founded by the Ministry of Development of Turkey (project code: DPT2006K – 120,470). Authors also acknowledge Zehra Aybegüm Ok for her support in *ex-situ* FTIR experiments.

Appendix A. Supplementary data

Supplementary material related to this article can be found, in the online version, at doi:https://doi.org/10.1016/j.apcatb.2019.118227.

References

[1] K. Skalska, J.S. Miller, S. Ledakowicz, Trends in NOx abatement: a review, Sci. Total Environ. 408 (2010) 3976–3989.
[2] U. Gehring, O. Gruzieva, R.M. Agius, R. Beelen, A. Custovic, J. Cyrys, M. Eeftens, C. Flexeder, E. Fuertes, J. Heinrich, B. Hoffmann, J.C. de Jongste, M. Kerkhof, C. Klumper, M. Korek, A. Molter, E.S. Schultz, A. Simpson, D. Sugiri, M. Svartengren, A. von Berg, A.H. Wijga, G. Pershagen, B. Brunekreef, Air pollution exposure and lung function in children: the ESCAPE project, Environ. Health Perspect. 121 (2013) 1357–1364.
[3] A. Folli, S.B. Campbell, J.A. Anderson, D.E. Macphee, Role of TiO2 surface hydration on NO oxidation photo-activity, J. Photochem. Photobiol. A: Chem. 220 (2011) 85–93.
[4] S. Roy, M.S. Hegde, G. Madras, Catalysis for NOx abatement, Appl. Energy 86 (2009) 2283–2297.
[5] S.M. Andonova, G.S. Şentürk, E. Ozensoy, Fine-tuning the dispersion and the mobility of BaO domains on NOx storage materials via TiO2 anchoring sites, J. Phys. Chem. C 114 (2010) 17003–17016.
[6] Z. Say, M. Tohumeken, E. Ozensoy, NOx storage and reduction pathways on zirconia and titania functionalized binary and ternary oxides as NOx storage and reduction (NSR) systems, Catal. Today 231 (2014) 135–144.
[7] Z. Say, O. Mihai, M. Kurt, L. Olsson, E. Ozensoy, Trade-off between NOx storage capacity and sulfur tolerance on Al2O3/ZrO2/TiO2–based $DeNO_x$ catalysts, Catal. Today 320 (2019) 152–164.
[8] G.P. Chossière, R. Malina, F. Allroggen, S.D. Eastham, R.L. Speth, S.R.H. Barrett, Country- and manufacturer-level attribution of air quality impacts due to excess NOx emissions from diesel passenger vehicles in Europe, Atmos. Environ. 189 (2018) 89–97.
[9] W.G. Lu, A.D. Olaitan, M.R. Brantley, B. Zekavat, D.A. Erdogan, E. Ozensoy, T. Solouki, Photocatalytic conversion of nitric oxide on titanium dioxide: cryo-trapping of reaction products for online monitoring by mass spectrometry, J. Phys. Chem. C 120 (2016) 8056–8067.
[10] M. Polat, A.M. Soylu, D.A. Erdogan, H. Erguven, E.I. Vovk, E. Ozensoy, Influence of the sol–gel preparation method on the photocatalytic NO oxidation performance of TiO2/Al2O3 binary oxides, Catal. Today 241 (2015) 25–32.
[11] D.A. Erdogan, M. Polat, R. Garifullin, M.O. Guler, E. Ozensoy, Thermal evolution of structure and photocatalytic activity in polymer microsphere templated TiO2 microbowls, Appl. Surf. Sci. 308 (2014) 50–57.
[12] A.M. Soylu, M. Polat, D.A. Erdogan, Z. Say, C. Yıldırım, Ö. Birer, E. Ozensoy, TiO2–Al2O3 binary mixed oxide surfaces for photocatalytic NOx abatement, Appl. Surf. Sci. 318 (2014) 142–149.
[13] R. Sugrañez, J.I. Álvarez, M. Cruz-Yusta, I. Mármol, J. Morales, J. Vila, L. Sánchez, Enhanced photocatalytic degradation of NOx gases by regulating the microstructure of mortar cement modified with titanium dioxide, Build. Environ. 69 (2013) 55–63.
[14] M.M. Ballari, H.J.H. Brouwers, Full scale demonstration of air-purifying pavement, J. Hazard. Mater. 254-255 (2013) 406–414.
[15] Q. Tay, X. Liu, Y. Tang, Z. Jiang, T.C. Sum, Z. Chen, Enhanced photocatalytic hydrogen production with synergistic two-phase Anatase/Brookite TiO2 nanostructures, J. Phys. Chem. C 117 (2013) 14973–14982.
[16] J. Lasek, Y.-H. Yu, J.C.S. Wu, Removal of NOx by photocatalytic processes, J. Photochem. Photobiol. C Photochem. Rev. 14 (2013) 29–52.
[17] J.Z. Bloh, A. Folli, D.E. Macphee, Photocatalytic NOx abatement: why the selectivity matters, RSC Adv. 4 (2014) 45726–45734.
[18] W.F. Schneider, Qualitative differences in the adsorption chemistry of acidic (CO2, SOx) and Amphiphilic (NOx) species on the alkaline earth oxides, J. Phys. Chem. B 108 (2004) 273–282.
[19] W.F. Schneider, K.C. Hass, M. Miletic, J.L. Gland, Dramatic cooperative effects in adsorption of NOx on MgO(001), J. Phys. Chem. B 106 (2002) 7405–7413.
[20] H. Grönbeck, P. Broqvist, I. Panas, Fundamental aspects of NOx adsorption on BaO, Surf. Sci. 600 (2006) 403–408.
[21] P.J. Schmitz, R.J. Baird, NO and NO2 adsorption on barium oxide: model study of the trapping stage of NOx conversion via lean NOx traps, J. Phys. Chem. B 106 (2002) 4172–4180.
[22] C.-W. Yi, J.H. Kwak, J. Szanyi, Interaction of NO2 with BaO: from cooperative adsorption to Ba(NO3)2 formation, J. Phys. Chem. C 111 (2007) 15299–15305.
[23] S. Andonova, Z.A. Ok, N. Drenchev, E. Ozensoy, K. Hadjiivanov, Pt/CeOx/ZrOx/γ-Al2O3 ternary mixed oxide $DeNO_x$ catalyst: surface chemistry and NOx interactions, J. Phys. Chem. C 122 (2018) 12850–12863.
[24] Z. Say, O. Mihai, M. Tohumeken, K.E. Ercan, L. Olsson, E. Ozensoy, Sulfur-tolerant BaO/ZrO2/TiO2/Al2O3 quaternary mixed oxides for $DeNO_X$ catalysis, Catal. Sci. Technol. 7 (2017) 133–144.
[25] E. Ozensoy, C.H.F. Peden, J. Szanyi, Low temperature H2O and NO2 coadsorption on θ-Al2O3/NiAl(100) ultrathin films, J. Phys. Chem. B 110 (2006) 8025–8034.
[26] E. Kayhan, S.M. Andonova, G.S. Şentürk, C.C. Chusuei, E. Ozensoy, Fe promoted NOx storage materials: structural properties and NOx uptake, J. Phys. Chem. C 114 (2010) 357–369.
[27] Z. Say, E.I. Vovk, V.I. Bukhtiyarov, E. Ozensoy, Influence of ceria on the NOx reduction performance of NOx storage reduction catalysts, Appl. Catal. B 142-143 (2013) 89–100.
[28] E. Ozensoy, D. Herling, J. Szanyi, NOx reduction on a transition metal-free γ-Al2O3 catalyst using dimethylether (DME), Catal. Today 136 (2008) 46–54.
[29] E. Ozensoy, C.H.F. Peden, J. Szanyi, NO2 adsorption on ultrathin θ-Al2O3 films: formation of nitrite and nitrate species, J. Phys. Chem. B 109 (2005) 15977–15984.
[30] E. Ozensoy, C.H.F. Peden, J. Szanyi, Model NOx storage systems: storage capacity and thermal aging of BaO/θ-Al2O3/NiAl(100), J. Catal. 243 (2006) 149–157.
[31] G. Busca, The surface acidity of solid oxides and its characterization by IR spectroscopic methods. An attempt at systematization, J. Chem. Soc. Faraday Trans. 1 (1999) 723–736.
[32] P.C. Hewlett, Lea's Chemistry of Cement and Concrete, Butterworth-Heinemann, 2003.
[33] M. Trueba, S.P. Trasatti, Γ-alumina as a support for catalysts: a review of fundamental aspects, Eur. J. Inorg. Chem. 2005 (2005) 3393–3403.
[34] L. Olsson, P. Jozsa, M. Nilsson, E. Jobson, Fundamental studies of NOx storage at low temperatures, Top. Catal. 42-43 (2007) 95–98.
[35] W.S. Epling, J.E. Parks, G.C. Campbell, A. Yezerets, N.W. Currier, L.E. Campbell, Further evidence of multiple NOx sorption sites on NOx storage/reduction catalysts, Catal. Today 96 (2004) 21–30.
[36] C. Verrier, J.H. Kwak, D.H. Kim, C.H.F. Peden, J. Szanyi, NOx uptake on alkaline earth oxides (BaO, MgO, CaO and SrO) supported on γ-Al2O3, Catal. Today 136 (2008) 121–127.
[37] T.J. Toops, D.B. Smith, W.S. Epling, J.E. Parks, W.P. Partridge, Quantified NOx adsorption on Pt/K/gamma-Al2O3 and the effects of CO2 and H2O, Appl. Catal. B 58 (2005) 255–264.
[38] J. Szanyi, J.H. Kwak, R.J. Chimentao, C.H.F. Peden, Effect of H2O on the adsorption of NO2on γ-Al2O3: an in situ FTIR/MS study, J. Phys. Chem. C 111 (2007) 2661–2669.
[39] K. Hadjiivanov, V. Bushev, M. Kantcheva, D. Klissurski, Infrared spectroscopy study of the species arising during nitrogen dioxide adsorption on titania (anatase), Langmuir 10 (1994) 464–471.
[40] R. Hummatov, O. Gülseren, E. Ozensoy, D. Toffoli, H. Üstünel, First-principles investigation of NOx and SOx adsorption on anatase-supported BaO and Pt overlayers, J. Phys. Chem. C 116 (2012) 6191–6199.
[41] L. Yang, A. Hakki, F. Wang, D.E. Macphee, Different roles of water in photocatalytic $DeNO_x$ mechanisms on TiO2: basis for engineering nitrate selectivity? ACS Appl. Mater. Interfaces 9 (2017) 17034–17041.
[42] Fine Ceramics (advanced Ceramics, Advanced Technical Ceramics) – Test Method for Air-purification Performance of Semiconducting Photocatalytic Materials – Part 1: Removal of Nitric Oxide, ISO 22197-1, 2007, pp. 1–11.
[43] J. Freitag, A. Domínguez, T.A. Niehaus, A. Hülsewig, R. Dillert, T. Frauenheim, D.W. Bahnemann, Nitrogen(II) oxide charge transfer complexes on TiO2: a new source for visible-light activity, J. Phys. Chem. C 119 (2015) 4488–4501.
[44] R.J. Lewis, Sax's Dangerous Properties of Industrial Materials, 11 ed., John Wiley & Sons, Inc., Hoboken, New Jersey, 2004.

[45] H. Kisch, D. Bahnemann, Best Practice in Photocatalysis: Comparing Rates or Apparent Quantum Yields? J. Phys. Chem. Lett. 6 (2015) 1907–1910.
[46] S. Sasol, PURALOX®/CATALOX® High Purity Activated Aluminas, (2018).
[47] A.M. Kalinkin, E.V. Kalinkina, O.A. Zalkind, T.I. Makarova, Chemical interaction of calcium oxide and calcium hydroxide with CO2 during mechanical activation, Inorg. Mater. 41 (2005) 1073–1079.
[48] S.M. Andonova, G.S. Şentürk, E. Kayhan, E. Ozensoy, Nature of the Ti − Ba interactions on the BaO/TiO2/Al2O3 NOx storage system, J. Phys. Chem. C 113 (2009) 11014–11026.
[49] O. Carp, C.L. Huisman, A. Reller, Photoinduced reactivity of titanium dioxide, Prog. Solid State Chem. 32 (2004) 33–177.
[50] L. Sivachandiran, F. Thevenet, P. Gravejat, A. Rousseau, Investigation of NO and NO2 adsorption mechanisms on TiO2 at room temperature, Appl. Catal. B 142-143 (2013) 196–204.
[51] J.A. Rodriguez, T. Jirsak, G. Liu, J. Hrbek, J. Dvorak, A. Maiti, Chemistry of NO2 on oxide surfaces: formation of NO3 on TiO2(110) and NO2↔O vacancy interactions, J. Am. Chem. Soc. 123 (2001) 9597–9605.
[52] Z. Say, M. Dogac, E.I. Vovk, Y.E. Kalay, C.H. Kim, W. Li, E. Ozensoy, Palladium doped perovskite-based NO oxidation catalysts: the role of Pd and B-sites for NOx adsorption behavior via in-situ spectroscopy, Appl. Catal. B 154-155 (2014) 51–61.
[53] Q.L. Yu, H.J.H. Brouwers, Indoor air purification using heterogeneous photocatalytic oxidation, Part I: Experimental study, Applied Catalysis B: Environmental 92 (2009) 454–461.
[54] G. Hüsken, M. Hunger, H.J.H. Brouwers, Experimental study of photocatalytic concrete products for air purification, Build. Environ. 44 (2009) 2463–2474.
[55] P.A. Thiel, T.E. Madey, The interaction of water with solid surfaces: fundamental aspects, Surf. Sci. Rep. 7 (1987) 211–385.
[56] M.A. Henderson, The interaction of water with solid surfaces: fundamental aspects revisited, Surf. Sci. Rep. 46 (2002) 1–308.
[57] M.A. Henderson, A surface science perspective on TiO2 photocatalysis, Surf. Sci. Rep. 66 (2011) 185–297.
[58] Z.-T. Wang, M.A. Henderson, I. Lyubinetsky, Origin of coverage dependence in photoreactivity of carboxylate on TiO2(110): hindering by charged coadsorbed hydroxyls, ACS Catal. 5 (2015) 6463–6467.
[59] G. Rubasinghege, V.H. Grassian, Role(s) of adsorbed water in the surface chemistry of environmental interfaces, Chem. Commun. 49 (2013) 3071–3094.
[60] V. Muñoz, C. Casado, S. Suárez, B. Sánchez, J. Marugán, Photocatalytic NOx removal: rigorous kinetic modelling and ISO standard reactor simulation, Catal. Today 326 (2019) 82–93.
[61] M. Hunger, G. Hüsken, H.J.H. Brouwers, Photocatalytic degradation of air pollutants — from modeling to large scale application, Cem. Concr. Res. 40 (2010) 313–320.
[62] D. Uner, I. Bayar, T. Tabari, The influence of relative humidity on photocatalytic oxidation of nitric oxide (NO) over TiO2, Appl. Surf. Sci. 354 (2015) 260–266.
[63] S. Devahasdin, C. Fan, K. Li, D.H. Chen, TiO2 photocatalytic oxidation of nitric oxide: transient behavior and reaction kinetics, J. Photochem. Photobiol. A: Chem. 156 (2003) 161–170.
[64] H. Wang, Z. Wu, W. Zhao, B. Guan, Photocatalytic oxidation of nitrogen oxides using TiO2 loading on woven glass fabric, Chemosphere 66 (2007) 185–190.
[65] C.H. Ao, S.C. Lee, Enhancement effect of TiO2 immobilized on activated carbon filter for the photodegradation of pollutants at typical indoor air level, Appl Catal B-Environ 44 (2003) 191–205.
[66] Y. Fujimori, X. Zhao, X. Shao, S.V. Levchenko, N. Nilius, M. Sterrer, H.-J. Freund, Interaction of water with the CaO(001) surface, J. Phys. Chem. C 120 (2016) 5565–5576.